BioSystems 202 (2021) 104354

Contents lists available at ScienceDirect

BioSystems

journal homepage: http://www.elsevier.com/locate/biosystems

Mixed-monolayer functionalized gold nanoparticles for cancer treatment: Atomistic molecular dynamics simulations study

Marina Kovacevic [a,*], Igor Balaz [b], Domenico Marson [c], Erik Laurini [c], Branislav Jovic [a]

[a] Department of Chemistry, Biochemistry and Environmental Protection, Faculty of Sciences, University of Novi Sad, Serbia
[b] Laboratory of Meteorology, Biophysics and Physics, University of Novi Sad, Serbia
[c] Molecular Biology and Nanotechnology Laboratory (MolBNL@UniTS), DEA, University of Trieste, Italy

ARTICLE INFO

Keywords:
Mixed-monolayer gold nanoparticles
Atomistic molecular dynamics simulation
Hydrophobicity
Nanomedicine
Cancer
Quinolinol
Panobinostat

ABSTRACT

Gold nanoparticles (AuNPs) are employed as drug carriers due to their inertness, non-toxicity, and ease of synthesis. An experimental search for the optimal AuNP design would require a systematic variation of physico-chemical properties which is time-consuming and expensive. Computational methods provide quicker and cheaper approach to complement experiments and provide useful guidelines. In this paper, we performed atomistic molecular dynamics simulations to study how the size, hydrophobicity, and concentration of the drug affect the structure of functionalized AuNPs in the aqueous environment. We simulated two groups of nano-systems functionalized with a zwitterionic background ligand, and a ligand carrying a drug (Quinolinol or Panobinostat). Results indicate that in the case of a hydrophobic drug (Quinolinol), the hydrophobicity drives the conformation changes of the coating layer. The tendency of the hydrophobic drug to reduce its solvent-accessible surface results in a decrease of the coating thickness and the overall NP size. Although the amount of accessible drug can be increased by increasing its initial concentration, it will compromise the solubility of the system. In the case of a hydrophilic drug (Panobinostat), the ligand in excess has a dominant influence on the final structure of the coating conformations. The percentage of accessible drug is significantly higher than in the hydrophobic systems for any given ratio. It implies that for hydrophilic systems we can generally expect higher biological efficiency. Our results highlight the importance of taking into account physico-chemical properties of drugs and ligands when developing gold-based nanosystems, especially in the case of hydrophobic drugs.

1. Introduction

The chemical properties of drugs can limit their distribution through the organism and cause various side effects (Peer et al., 2007). The use of nanoparticles (NP) as drug carriers can overcome those limitations and improve conventional anticancer treatments (Fanciullino, 2013; Van der Meel, 2019). Due to NP's versatility and possibilities of customization, they can improve site-specific targeting of drugs, increase *in vivo* stability, extend the drug's blood circulation time, and allow for controlled drug release (Maeda et al., 2013; Blanco et al., 2015; Wicki et al., 2015). NPs are also generally associated with less systemic toxicity compared to classical formulations, mainly by modifying the pharmacokinetic and pharmacodynamic properties of the drugs which they carry (Shi et al., 2017).

Among the wide range of different materials, gold nanoparticles (AuNPs) have been extensively exploited for drug delivery, targeting, and bioimaging due to their desirable properties (Fratoddi et al., 2015; Kumar et al., 2013). AuNPs are inert and non-toxic. They can easily be synthesized in various shapes and sizes. Multivalent surface structures of AuNPs and high surface-to-volume ratio provide the opportunity to incorporate multiple ligands and multiple ligand types. This functionalization, however, creates a monolayer coating that alters the physico-chemical properties of the surface. Therefore, the behavior of functionalized AuNPs is dominated not by the gold core itself, but by the properties of monolayer coating. By using molecules with specific characteristics, surface properties can be tuned to control biocompatibility, biodistribution, induce preferential interactions between ligands, adjust the charge density, etc. (Haume et al., 2016a; Rana et al., 2012; Marson et al., 2019; Van Lehn et al., 2013a).

The design of novel and efficacious nanomedicines requires a thorough understanding of their physico-chemical properties and how those properties determine their behavior in biological systems (Burello and

* Corresponding author.
E-mail address: marinak@dh.uns.ac.rs (M. Kovacevic).

https://doi.org/10.1016/j.biosystems.2021.104354
Received 31 August 2020; Received in revised form 23 December 2020; Accepted 5 January 2021
Available online 11 January 2021

Worth, 2011; Ramezanpour et al., 2016). However, experimentally determining all those properties can often be difficult since direct measurements are not always precise or possible. Additionally, although it has been shown that properties such as shape, size, surface coating, etc. significantly influence NPs biological effect it has not yet been established exactly in what manner. Moreover, creating "one perfect solution" is not feasible since the choice of the appropriate properties depends on the physiological target, mechanism of action for the chosen drugs, and intended functionality of the NP (Zhu et al., 2012). Experimental search for optimal NP design would required systematic variation of physico-chemical properties which is time-consuming and expensive. Therefore, there has been a lot of focus on the use of computational methods to study such systems (Vukovic et al., 2013; Heikkila et al., 2012; Van Lehn et al., 2013b; Stillman et al., 2020; Haume et al., 2016b). Understanding, on a molecular level, which properties or combination of properties determine the coating structure can give us more control over the final product and lead to a more efficient design of nanomedicines.

To optimally design AuNPs for medical applications, in terms of both drug accessibility and synthesis feasibility, the best solution would be to strive for the maximum concentration of the drug accessible to the solvent relative to the overall concentration of the drug attached to the nanoparticle. Additionally, a functionalized nanoparticle has to be soluble under physiological conditions. One more important aspect to keep in mind is "stealth". Since protein corona forms almost instantly when a drug is injected, appropriate ligands can be attached in order to minimize non-specific protein interactions (Barui et al., 2019). In this paper, atomistic molecular dynamics simulations were performed to study how the size, hydrophobicity, and concentration of the drug in the system affect the structure of functionalized nanoparticles in the aqueous environment. Drugs used in these experiments (Quinolinol and Panobinostat), were chosen based on their physico-chemical properties under the assumption that hydrophobic nature of Quinolinol and hydrophilic nature of Panobinostat will be comparable to other drugs with similar properties.

2. Methodology

2.1. System preparation

We simulated AuNPs functionalized with two types of thiolated ligands: a) one carrying the covalently bound anticancer drug (API-active pharmaceutical ingredient) and b) the zwitterionic background ligand (BL) (Fig. 1). We chose zwitterionic BL since it has been shown that they have a wide range of useful properties such as balancing surface charge, increasing the blood circulation time, having higher ionic solvation with water molecules, reducing protein adsorption, etc. (Fam et al., 2020; Chapman, 2000; Moreadith et al., 2017).

We modeled two types of systems (Fig. 1):

1) Gold nanoparticle functionalized with API carrying a small hydrophobic drug Quinolinol (API-Q) and zwitterionic background ligand (BL), and
2) Gold nanoparticle functionalized with API carrying a large hydrophilic Panobinostat (API-P) and zwitterionic background ligand (BL).

To ensure that all differences in the coating structure are exclusively a result of the drug's physico-chemical properties, the size of gold cores (5.5 nm), API ligands carrying the drugs, and BL were identical in both systems. We only varied ratios of the ligands, to test the effect of minor composition changes.

Gold nanoparticle (AuNP) cores have been modeled by arranging Au atoms on a fcc lattice into the icosahedral shape using OPENMD software (v. 2.3) (Bhattarai et al.; Fleury et al., 2015).

Ligand structures were uploaded to RED server to procure molecular electrostatic potential-based charges following the RESP procedure (Vanquelef et al., 2011). Parameterization of the ligands was then performed with AMBER's tleap program using the General Amber force

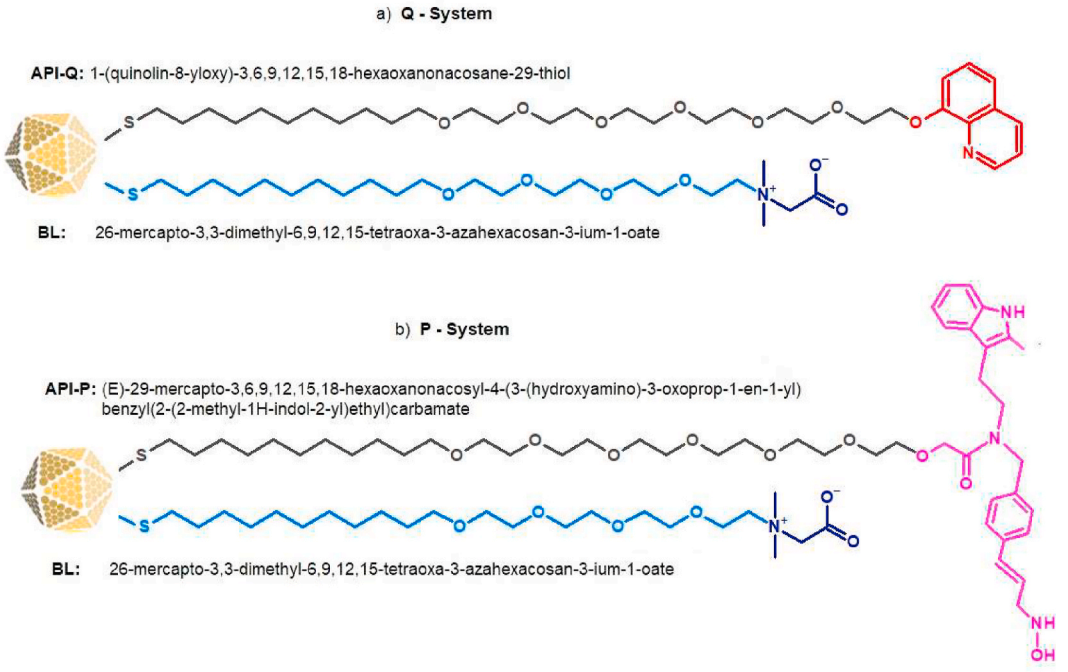

Fig. 1. Structures of ligands for AuNP functionalization: a) **Quinolinol system:** API-Q (1-(quinolin-8-yloxy)-3,6,9,15,18-hexaoxanonacosane-29-thiol), BL: (26-mercapto-3,3-dimethyl-6,9,12,15-tetraoxa-3azahexacosan-3-ium-1-oate); b) **Panobinostat system:** API-P ((E)-29-mercapto-3,6,9,12,15,18-hexaoxanonacosyl-4-(3-hydroxyamino)-3-oxoprop-1-en-1-yl)benzyl(2-(2-methyl-1*H*-indol-2-yl)ethyl)carbamate), BL: (26-mercapto-3,3-dimethyl-6,9,12,15-tetraoxa-3azahexacosan-3-ium-1-oate). API ligand is colored grey with the different colors for terminally attached drug molecules – red for Quinolinol and pink for Panobinostat. In every snapshot background ligand (BL) is colored light blue with the terminal zwitterionic ligand colored dark blue. The same coloring scheme is used in Figs. 2, 5 and 6. (For interpretation of the references to color in this figure legend, the reader is referred to the Web version of this article.)

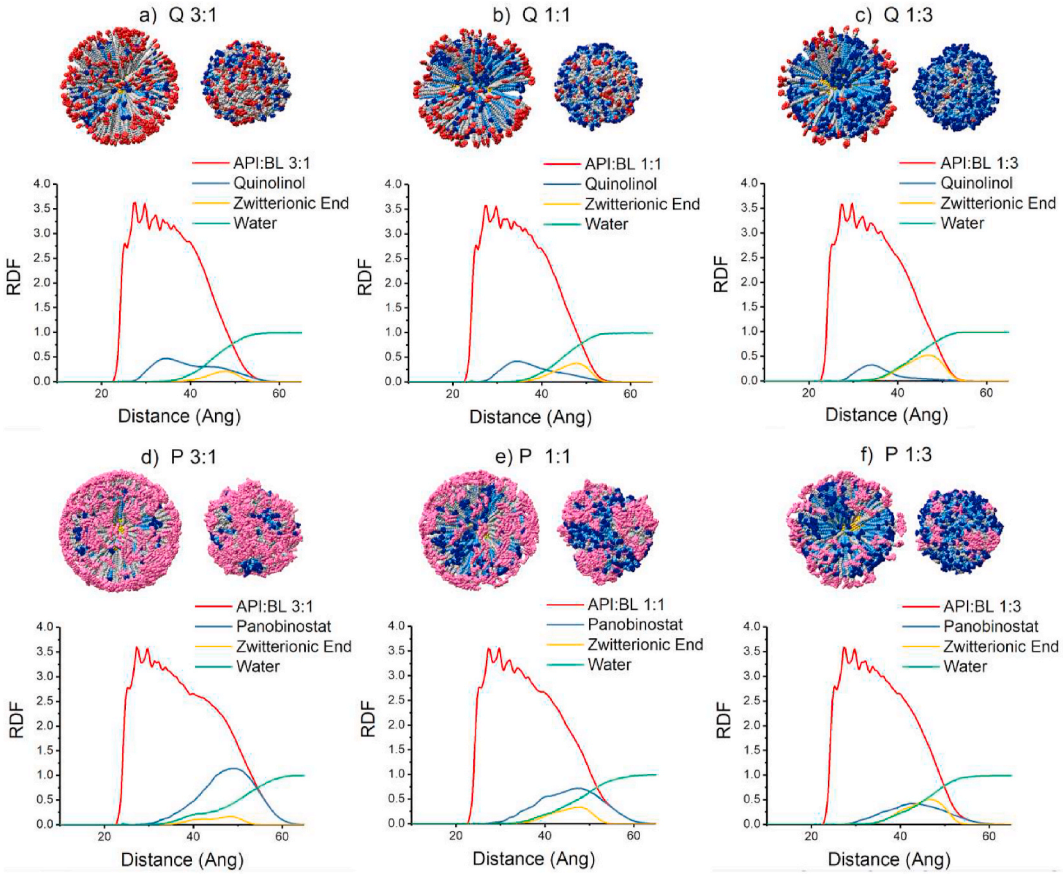

Fig. 2. RDF plots and Simulations snapshots. Simulation snapshots: In each panel, the first frame shows ligands completely extended before equilibration while the last frame shows the equilibrated structure of the nanoparticle with bended ligands. Below both frames are the corresponding RDF graphs. API ligand is colored grey with the different colors for terminally attached drug molecules – red for Quinolinol and pink for Panobinostat. In every snapshot background ligand (BL) is colored light blue with the terminal zwitterionic ligand colored dark blue. Water is not shown for clarity. First row (left to right): API (Quinolinol):Background ligand ratio 3:1, 1:1, and 1:3, respectively. Second row (left to right) API (Panobinostat):Background ligand ratio 3:1, 1:1, and 1:3. (RDFs for other ratios can be found in the supplementary material). (For interpretation of the references to color in this figure legend, the reader is referred to the Web version of this article.)

field (Case et al., 2020; Wang et al., 2004). Systems were assembled and AuNPs were functionalized each with 420 ligands using Packmol (Martinez et al., 2009) software to ensure maximum homogenous surface coverage. Ligand density was approximated to 5 ligands per nm^2.

A flat-wall potential was used, starting acting at a distance of 2 Å from the gold surface on any sulfur atoms (harmonic spring constant of 10 kcal/mol), to ensure that no ligand can escape from the AuNP. This potential was chosen to allow the ligands to freely move on the surface of the AuNP, starting from the random arrangement of ligands obtained from Packmol.

Prepared ratios of API:BL for both systems were: 3:1, 2:1, 1:1, 1:2, and 1:3.

(For easier identification, in the following text systems containing Panobinostat are labeled as "P", and Quinolinol as "Q" followed by the numbers which depict the ratios of API:BL. For example, P3:1 describes AuNP functionalized with API carrying Panobinostat and zwitterionic background ligand, where the ratio of API:BL ligand is 3:1).

Functionalized NPs were solvated with TIP3 water molecules (Jorgensen et al., 1983), extending at least 12.0 Å from each solute atoms.

To prepare molecular systems, visualize trajectories, and prepare images we used UCSF Chimera (Pettersen et al., 2004) and Avogadro (Hanwell et al., 2012).

2.2. MD simulations

For all molecular dynamics simulations, we used AMBER19. Before the actual simulations, we minimized the energy of the systems to adjust the initial structure to the force field and to relax possible steric clashes. First, we applied Steepest Descent/Conjugated Gradient minimization with restraints on the solute (5.0 kcal/(mol*A^2)). It was followed by the minimization without restraints to make sure that all bad contacts are eliminated. Then the system was gradually heated to 300K in the canonical ensemble. The temperature was controlled using Langevin Thermostat with a collision frequency of 1.0 ps^{-1}. To equilibrate the density of the water box, we switched to isothermal-isobaric ensemble while holding the restraint on the solute. The pressure was controlled by using a Berendsen barostat. In the following step, restraints were gradually removed and the systems were equilibrated in the NPT ensemble for 8 ns. Pressure control was exerted by coupling the system to a Berendsen barostat. Timestep was 2 fs. Systems were equilibrated for an additional 5ns using Monte Carlo (MC) barostat. The production phase was run for 300 ns where pressure control was exerted by coupling the system to MC barostat. The SHAKE algorithm was applied to all covalent bonds involving hydrogen atoms. Electrostatic interactions were simulated with the particle mesh Ewald (PME) with a direct cut-off of 10 $Å^{2.}$. All simulations were performed on Puhti supercomputer (CSC data center in Kajaani, Finland).

2.3. Data analysis

Data analyses in this paper were carried out using the cpptraj program of AMBER19, VMD1.9.3 (Humphrey et al., 1996), and custom-developed Python scripts.

The radial distribution function (RDF) was calculated as a function

of the distance from the center of mass of the AuNP core. **Solvent Accessible Surface Area** (SASA, probe radius set to 1.4 Å) was calculated for i) the entire system, ii) drug molecules, and iii) the zwitterionic terminal end of the background ligand. Separate calculations for the drug molecules and terminal end were performed to determine the influence of these fragments in the overall composition since the rest of the ligand structures are identical.

The percentage of **accessible drug molecules** for equilibrated systems was calculated as a ratio of a drug's SASA to the total theoretical accessible area of the same drug molecule. We calculated two nanoparticle size values, before and after the simulations. **The measured size of the functionalized nanoparticle** (d_m) was determined from the simulations as the average distance between the center of the mass of the Au core and the terminal groups (Heikkila et al., 2012). Obtained d_m **values are compared to the nanoparticle size before the simulations** (d_{ext}), calculated as the average distance between the center of mass of the Au core and averaged lengths of extended ligands. **Measured average coating thickness** (CT) was calculated after the simulations as the thickness which contained 97% of the coating atoms measured from the gold surface (Haume et al., 2016a). **End-to-end distance** (<Rs-n>) was calculated before the simulations as the average distance from the position of the sulfur atoms to the terminal end of the completely extended ligands (Haume et al., 2016a).

3. Results and discussion

3.1. HYDROPHOBIC vs. HYDROPHILIC DRUG

Here we compare how small hydrophobic drug Quinolinol and large, highly hydrophilic drug Panobinostat affect the mixed-monolayer coating.

For both Q and P-systems, regardless of the different API:BL ratio (Fig. 2) we can observe the same trend – higher initial concentration of the drug correlates with the higher amount of the drug available on the surface. However, in the case of Quinolinol, BL remains dominant on the surface for all tested ratios (Fig. 2 a-c). This trend is visible from provided snapshots but is also confirmed by RDFs (Fig. 2), where the average density of Quinolinol is closer to the AuNP surface than the average Panobinostat density.

This difference can be explained by the hydrophobicity of the Q-system. From Fig. 1 can be seen that API ligand carrying the drug is flexible. It is confirmed by RDF where ligand peaks are quite broad (Fig. 2), which refers to their flexibility. Since Quinolinol is hydrophobic, it tends to decrease its surface in contact with the polar solvent. This is achieved by bending the flexible API-Q ligand towards the AuNP core. At the same time, polar BL extends towards the solvent covering the drug underneath the surface. On the other hand, Panobinostat is hydrophilic, thus does not need to "hide away" from the aqueous environment.

Bending of the ligands also influences overall NP size and coating thickness (Table 1 and 2.). Deviations of the measured size after the simulations (d_m) from d_{ext} (Table 1) increase with a higher API to BL ratio. This indicates that the discrepancy is due to the bending of the API and not the background ligands.

A similar trend can be observed by comparing the values of coating thickness before (<Rs-n>) and after the simulations (CT)(Table 2). Deviations are higher in the case of Quinolinol which implies that bending of API ligands is more prominent in API ligands carrying the hydrophobic drug.

When evaluating water penetration into the coating (Fig. 3) we can see that in Q-systems water can get closer to the gold surface than in the P-systems. Although it would be reasonable to assume that more water molecules could penetrate in the case of hydrophilic Panobinostat, it does not happen in our simulations. A possible explanation could be steric effects due to the voluminosity of the Panobinostat molecule, and the higher polarity of the zwitterionic BL. Due to their higher polarity, zwitterions have a higher affinity for the polar solvent. Consequently, they tend to extend towards the solvent while causing API-P to bend in opposite direction: away from the solvent and towards the gold surface, although to a much lesser degree compared to the Quinolinol system. API-P also has limited rotation around its central amide nitrogen atom (Fig. 1b), so higher rigidity and sheer size of the Panobinostat may prevent water from penetrating deeper in the coating.

Deeper water penetration for Q-system is explained above. Since API-Q ligands bend towards the gold surface, a more hydrophilic part of the chain becomes exposed to the solvent allowing water molecules to approach.

SASA has been calculated separately for a) the entire functionalized nanoparticle (overall SASA), b) just the for drug, and c) zwitterionic terminal end of the BL (Fig. 4). The main difference between Q and P-systems is that the overall SASA for Q-systems increases with the increase of the BL concentration, while overall SASA for P-systems shows the opposite trend. This is again explained by the drug hydrophobicity and ligand flexibility. Hydrophobic API-Q ligands bend towards the gold surface while polar BL behaves in an exactly opposite manner by extending towards the solvent and increasing the solubility of the system. Therefore, adding more BL into the Q-system increases the overall SASA. On the other hand, Panobinostat is a large, hydrophilic molecule whose large surface area is responsible for higher SASA. By increasing the ratio of BLs, we decrease the overall size and surface, and as a consequence decrease overall SASA. In both systems, SASA of the zwitterionic terminal end increases with its concentration. This is expected due to the polarity of the BL.

Table 3 shows the percentage of the solvent accessible drug for each system. Values in the table show that regardless of the API:BL ratio, the percentage of accessible Panobinostat is significantly higher than the percentage of accessible Quinolinol (detailed explanation will be given in Section 4).

4. Varying ratios

Here we compare the results within each group of simulations. As mentioned above, for both Q and P-systems additional simulations were performed where ratios of API:BL were varied. By doing so, we can assess to what extent the relative amount of ligands influences the final structure.

4.1. Quinolinol systems

First, we discuss varying ratios for the API-Q:BL system (Q3:1, Q2:1, Q1:1, Q1:2, Q1:3). RDF analysis shows that the overall coating density distribution does not differ significantly among the systems (Fig. 5). In the case of the zwitterionic terminal end,the highest density remains around 55 Å. The area under the curve increases proportionally with the increase in the BL concentration. However, that is not the case for the drug. With decreasing drug concentration, drug density is shifting slightly closer to the gold surface. On the other hand, when the drug

Table 1
Average size of functionalized nanoparticles.

Average NP size	Q3:1	Q2:1	Q1:1	Q1:2	Q1:3	P3:1	P2:1	P1:1	P1:2	P1:3
d_m (Å)	120	120	120	119.5	119.5	128.5	127.5	127	126.5	126
d_{ext}(Å)	132.4	131.1	128.5	125.9	124.5	141.4	139.1	134.5	129.8	127.6
Deviation of d_m from d_{ext}(Å)	12.4	11.1	8.5	6.4	5	12.9	11.6	7.5	3.3	1.6

Table 2
Average Coating thickness and average end-to-end distance calculated for extended ligands (<Rs-n>).

Average (Å)	Q3:1	Q2:1	Q1:1	Q1:2	Q1:3	P3:1	P2:1	P1:1	P1:2	P1:3
CT	23.75	24.25	23.25	22.75	22.75	34.00	34.00	33.00	30.00	29.50
<Rs-n>	38.71	38.05	36.74	35.43	34.77	43.22	39.33	39.75	37.44	33.55
Deviation from <Rs-n>	14.96	13.80	13.49	12.68	12.02	9.22	5.33	6.75	7.44	4.05

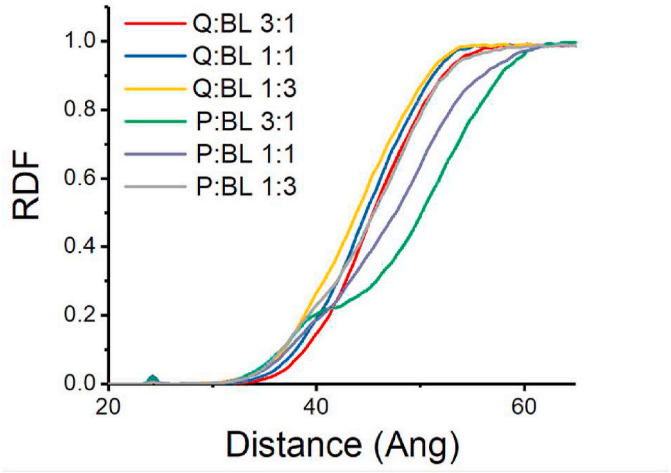

Fig. 3. RDF plot of water for simulated systems.

concentration increases RDF peaks broaden and the new "maximum" is closer to the solvent. Simulation snapshots (Fig. 5) are in agreement with these observations. Overall it is obvious that BLs tend to "cover" hydrophobic drug. For lower drug concentrations (e.g. Q:BL 1:2, Q:BL 1:3), the surface in contact with solvent is almost completely composed of BLs. However, for systems with higher drug concentration, a certain amount of API-Q starts to appear on the surface despite its hydrophobicity. A possible reason could be that bent ligands occupy more volume near the gold surface than their extended counterparts. Thus, with an increase in API-Q concentration, there is not enough free volume for all ligands near the gold surface. As a result, some of them are forced to extend outwards. Additionally, although polar BL tends to cover the hydrophobic drug, at lower BL concentrations this would not be possible.

How does the API:BL ratio influences the depth of water penetration into the coating is shown in Fig. 3. Water penetration increases in the following order: Q3:1<Q2:1<Q1:1<Q1:2<Q1:3. An explanation of the overall mechanism is given in Section 3. Since bent API-Q ligands occupy more volume than their extended counterpart, a lower concentration of API-Q can "leave" sufficient volume for water molecules to

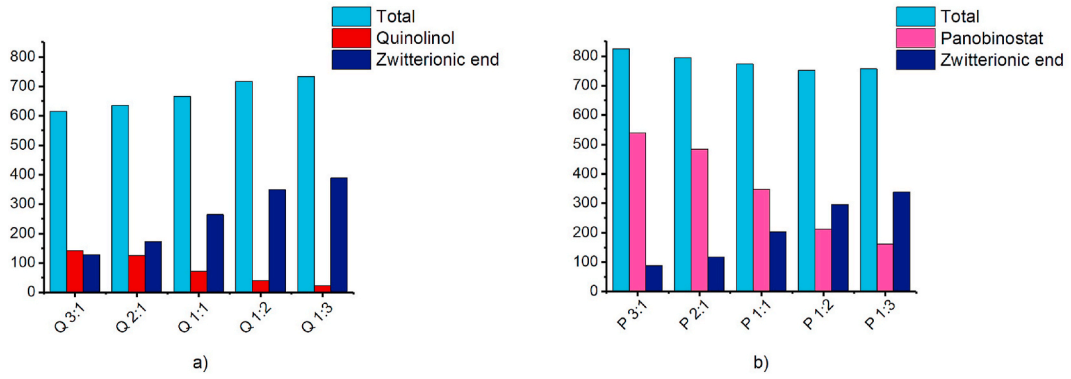

Fig. 4. Solvent Accessible Surface Area. a) API-Q/BL: Q3:1, Q2:1, Q1:1. Q1:2, Q1:3 b) API-P/BL: P3:1. P2:1. P1:1. P1:2, P1:3.

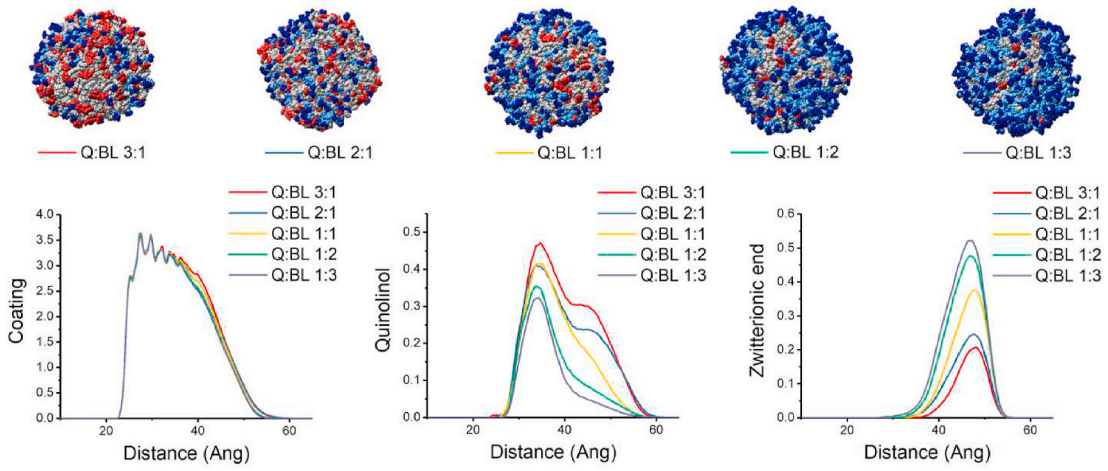

Fig. 5. Simulation snapshots of equilibrated structures for systems with API-Q:BL ratios 3:1, 2:1, 1:1, 1:2, 1:3 and RDF plots. RDF plots from left to right: Overall RDF, RDF of Quinolinol, RDF of zwitterionic terminal end of the background ligand.

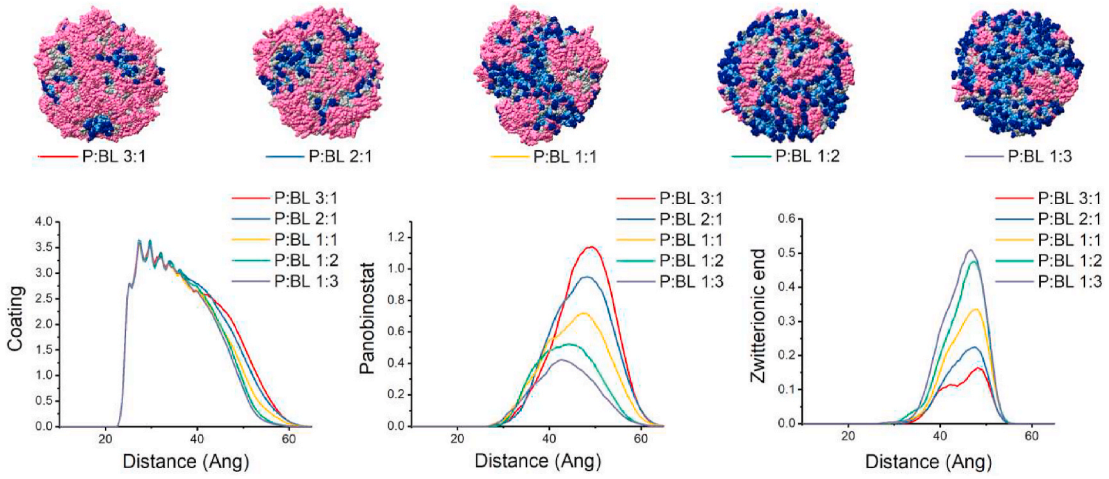

Fig. 6. Simulation snapshots of equilibrated structures for systems with API-P:BL ratios 3:1, 2:1, 1:1, 1:2, 1:3 and RDF plots. RDF plots from left to right: Overall RDF, RDF of Panobinostat, RDF of zwitterionic terminal end of the background ligand.

pass through. By increasing the API-Q concentration hydrophobic area also increases, thus not allowing water to get closer. This indicates that the depth to which water can penetrate into the coating is determined by the ratios of API to BL.

Change of API-Q:BL ratios also influences the measured coating thickness - CT (Fig. 7). Decreasing API-Q concentration leads to a slight CT decrease until it became stable for low API-Q:BL ratios. This relative stability can be explained by the small amount of API-Q that can bend toward the surface without disturbing the overall conformation of BL ligands which extended almost completely to the solvent. If this is the case, BL has a dominant role in defining the surface of the functionalized NP in Q-system. As expected from the previous discussion, CT significantly deviates from the values obtained before the simulations.

To assess the total "yield of the useable drug" we have also calculated the percentage of the drug surface accessible to the solvent (Table 3). In the case of hydrophobic Quinolinol, the overall "yield" is quite low reaching just over 20% even at the highest API-Q:BL ratio (3:1). This percentage would be difficult to increase further without compromising the solubility of the system.

4.2. Panobinostat systems

Here, we discuss varying ratios for the API-P:BL system (P3:1, P2:1, P1:1, P1:2, P1:3).

In the group of Panobinostat simulations, peaks on the overall RDF plot (Fig. 6) become broader with the increase of concentration of API ligands. It also leads to increase of coating thickness as well as of the amount of drug accessible to the solvent (Tables 2 and 3; Fig. 3). This is also evident from the simulation snapshots. Due to the size of the drug it is possible that with increasing API-P concentration, ligands are forced to distribute away from the gold surface to avoid steric clashes. On RDF plots of Panobinostat and zwitterions we can see that with decreasing the API-P concentration, the Panobinostat peak broadens and shifts toward the AuNP surface which indicates its flexibility, whereas the peak of the zwitterions shifts towards the solvent.

An explanation for this would be that zwitterions are more polar and have a higher affinity for the solvent so they extend outward, and the concentration of the drug is relatively low so it can slightly bend and distribute in such a way not to cover the BL. With a higher concentration of Panobinostat, due to the longer chain and large drug size, API ligands tend to cover the surface in contact with water, pressuring the BL to adjust under it. This can be observed from the RDF plots for a higher concentration of the drug and a lower concentration of the BL. This is also reflected in the coating thickness (Fig. 7). Measured coating thickness deviates from the <Rs-n> values, but to a much lower degree than in the case of Quinolinol. This may be due to the higher polarity of the zwitterionic BL. Although coating thickness should decrease proportionately to API concentration, from the simulation results we can see that is not happening. In the range of ratios from 2:1 to 1:2 both coating thickness and drug accessibility change drastically, but increasing or decreasing the drug concentration beyond those values does not have a notable influence on the overall structure. With higher

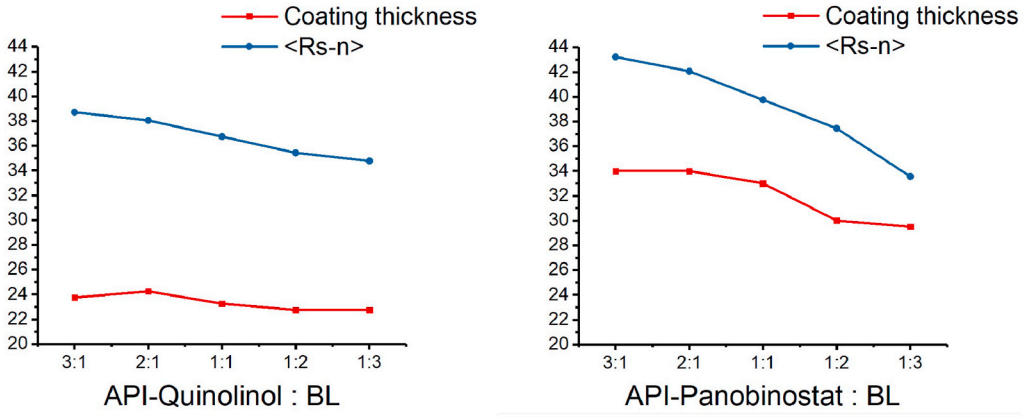

Fig. 7. Comparison of calculated average End-to-end distance <Rs-n> and Average Coating Thickness obtained from the simulations.

Table 3
Percentage of drug surface accessible to the solvent, after equilibration.

DRUG	Q3:1	Q2:1	Q1:1	Q1:2	Q1:3	P3:1	P2:1	P1:1	P1:2	P1:3
%	20.81	20.14	14.41	11.64	8.74	52.84	49.35	43.28	36.09	34.41

API concentrations Panobinostat has a dominant influence on the resulting structure, whereas the opposite is true for the higher BL concentrations.

Similar to Quinolinol systems, the amount of drug accessible to the solvent increases with increasing API-P concentration (Table 3). An important thing to note is that, unlike Q-systems, the "yield" of the accessible drug is much higher in Panobinostat systems for each tested ratio. While for Q-systems maximal achieved "yield" is just over 20%, for the hydrophilic Panobinostat much higer percentage is already achieved at the smallest tested ratio (P1:3), and goes up to almost 53% (P3:1).

5. Conclusion

We performed atomistic molecular dynamics simulations of 10 different functionalized gold nanoparticles to study how distinct physico-chemical properties of drugs used for functionalization, influence the structure of the coating layer.

AuNPs were functionalized with API ligands (carrying either the small hydrophobic drug Quinolinol or large hydrophilic drug Panobinostat) and zwitterionic background ligands. Simulations were performed for different ratios of these ligands.

Our results show that for Quinolinol systems, the hydrophobicity of the drug has the main influence on the coating structure in an aqueous environment. The tendency of the hydrophobic drug to decrease its surface accessible to the polar solvent results in a decrease in NP size and coating thickness. The solubility of the system increases proportionally with an increase in BL concentration. Therefore, to overcome the issue of solubility, hydrophilic BL can be added to the system. However, by doing so, the amount of the solvent-accessible drug decreases significantly. This implies that the initial concentrations of the API and BL also have a role in determining structure in aqueous, and by extension, biological environment. By varying the ratio of these ligands, balance can be shifted. But there is an obvious limit. Although the amount of the accessible drug can be increased by increasing initial API concentration, the solubility of the system can be compromised or completely lost.

In the case of a hydrophilic drug, the ligand in excess has a dominant influence on the final coating conformations. If the API-P is in excess, due to its size and voluminosity, it extends and covers the surface pressuring the BL to bend and occupy availably area beneath. If the BL is in excess, due to its higher polarity, it similarly influences the API conformation. The percentage of the solvent-accessible drug is significantly higher than in the hydrophobic systems for any given ratio. This is expected due to the overall hydrophilic nature of the P-system. This implies that higher efficiency for the hydrophilic system can be expected as well.

Our results indicate that one should be cautious with the choice of the drug for the functionalization. Relying only on the drug's pharmacology is not enough. Physico-chemical properties of a drug and background ligands are of equal importance. We also call into question the usefulness and practicality of using hydrophobic drugs with these types of nanoparticles, although additional conformational experiments are needed. The results also show the importance of performing simulations before synthesis. They can provide important guidelines for efficient design and eliminate potentially unsuccessful ones, thus saving resources and speeding up the process of producing new nanomedicines.

Declaration of competing interest

Hereby we confirm that none of the authors of this paper has a financial, personal or other relationship with other people or organizations that could inappropriately influence or be perceived to influence the content of the paper.

Acknowledgements

This project has received funding from the European union's Horizon 2020 research and innovation programme under grant agreement No 800983.

This article/publication is based upon work from COST Action CA 17140 "Cancer Nanomedicine from the Bench to the Bedside" supported by COST (European Cooperation in Science and Technology). We are thankful to prof. Sabrina Pricl for her crucial assistance during the planning and development of this manuscript.

We are thankful to ProChimia Surfaces for providing ligand structures and to Dr. Sébastien Lafond, Dr. Sepinoud Azimi and Dr. Vid Sustar from ÅboAkademi University, Finland for their help in running the simulations. The authors wish to acknowledge CSC – IT Center for Science, Finland, for computational resources.

Appendix A. Supplementary data

Supplementary data to this article can be found online at https://doi.org/10.1016/j.biosystems.2021.104354.

References

Barui, A.K., et al., 2019. Cancer-Targeted nanomedicine: overcoming the barrier of the protein corona. Advanced Therapeutics 3, 1900124.
Bhattarai, H., et al.. OPENMD, an open source engine for molecular dynamics. http://openmd.net.
Blanco, E., et al., 2015. Principles of nanoparticle design for overcoming biological barriers to drug delivery. Nat. Biotechnol. 33, 941–951.
Burello, E., Worth, A.P., 2011. QSAR modeling of nanomaterials. Wiley Interdiscip. Rev.: Nanomedicine and Nanobiotechnology 3, 298–306.
Case, D.A., et al., 2020. AMBER 2020. University of California, San Francisco.
Chapman, R.G., 2000. Surveying for surfaces that resist the adsorption of proteins. J. Am. Chem. Soc. 122, 8303–8304.
Fam, S., et al., 2020. Stealth coating of nanoparticles in drug-delivery systems. Nanomaterials 10, 787.
Fanciullino, R., 2013. Challenges, expectations and limits for nanoparticles-based therapeutics in cancer: a focus on nano-albumin-bound drugs. Crit. Rev. Oncol. Hematol. 88, 504–513.
Fleury, B., et al., 2015. Gold nanoparticle internal structure and symmetry probed by unified small-angle X-ray scattering coupled with molecular dynamics analysis. Nano Lett. 15, 6088–6094.
Fratoddi, I., et al., 2015. How toxic are gold nanoparticles? The stat of the art. Nano Research 8, 1771–1799.
Hanwell, M.D., et al., 2012. Avogadro: an advanced semantic chemical editor, visualization, and analysis platform. J. Cheminf. 4, 17.
Haume, K., et al., 2016a. Modeling of nanoparticle coatings for medical applications. The European Physical Journal D 70, 181.
Haume, K., et al., 2016b. Modeling of nanoparticle coatings for medical applications. The European Physical Journal D 70, 181.
Heikkila, E., et al., 2012. Atomistic simulations of functional $Au_{144}(SR)_{60}$ gold nanoparticles in aqueous environment. J. Phys. Chem. C 116, 9805–9815.
Humphrey, W., et al., 1996. Vmd – visual molecular dynamics. J. Mol. Graph. 14, 33–38.
Jorgensen, W.L., et al., 1983. Comparison of simple potential functions for simulating liquid water. J. Chem. Phys. 79, 926–935.
Kumar, A., et al., 2013. Gold nanoparticles: emerging paradigm for targeted drug delivery system. Biotechnol. Adv. 31, 593–606.
Van Lehn, R.C., et al., 2013a. Structure of mixed-monolayer-protected nanoparticles in aqueous salt solution from atomistic molecular dynamics simulations. J. Phys. Chem. C 117, 20104–20115.
Van Lehn, R.C., et al., 2013b. Effect of particle and surface composition on the spontaneous fusion of monolayer-protected gold nanoparticles with lipid bilayers. Nano Lett. 13, 4060–4067.
Maeda, H., et al., 2013. The EPR effect for macromolecular drug delivery to solid tumors: improvement of tumor uptake, lowering of systemic toxicity, and distinct tumor imaging in vivo. Adv. Drug Deliv. Rev. 65, 71–79.

Marson, D., et al., 2019. Mixed fluorinated/hydrogenated self-assembled monolayer-protected gold nanoparticles: in silico and in vitro behaviour. Small 1900323.
Martinez, L., et al., 2009. Packmol: a package for building initial configurations for molecular dynamics simulations. J. Comput. Chem. 30, 2157–2164.
Van der Meel, R., 2019. Smart cancer nanomedicine. Nat. Nanotechnol. 14, 1007–1017.
Moreadith, R.W., et al., 2017. Clinical development of a poly(2-oxazoline) (POZ) polymer therapeutic for the treatment of Parkinson's disease – proof o concept of POZ as a versatile polymer platform for drug development in multiple therapeutic indications. Eur. Polym. J. 88, 524–552.
Peer, D., et al., 2007. Nanocarriers as an emerging platform for cancer therapy. Nat. Nanotechnol. 2, 751–760.
Pettersen, E.F., et al., 2004. UCSF Chimera – a visualization system for exploratory research and analysis. J. Comput. Chem. 13, 1605–1612.
Ramezanpour, M., et al., 2016. Computational and experimental approaches for investigating nanoparticle-based drug delivery systems. BiochimicaetBiophysicaActa – Biomembranes 7, 1688–1709.
Rana, S., et al., 2012. Monolayer coated gold nanoparticles for delivery applications. Adv. Drug Deliv. Rev. 64, 200–216.
Shi, J., et al., 2017. Cancer nanomedicine: progress, challenges and opportunities. Nat. Rev. Canc. 17, 20–37.
Stillman, N., et al., 2020. In silico modelling of cancer nanomedicine, across scales and transport barriers. npj Computational Materials 6, 92.
Vanquelef, E., et al., 2011. R.E.D. Server: a web service for deriving RESP and ESP charges and building force field libraries for new molecules and molecular fragments. Nucleic Acids Res. 39, W511–W517.
Vukovic, L., et al., 2013. Solubilization of therapeutic agents in micellar nanomedicines. Langmuir 29, 15747–15754.
Wang, J., et al., 2004. Development and testing of a general amber force field. J. Comput. Chem. 25, 1157–1174.
Wicki, A., et al., 2015. Nanomedicine in cancer therapy: challenges, opportunities, and clinical applications. J. Contr. Release 28, 138–157.
Zhu, M., et al., 2012. Physicochemical properties determine nanomaterial cellular uptake, transport, and fate. Acc. Chem. Res. 46 (3), 622–631.